AIAA JOURNAL
Vol. 47, No. 8, August 2009

External Mean Flow Influence on Noise Transmission Through Double-Leaf Aeroelastic Plates

F. X. Xin,* T. J. Lu,† and C. Q. Chen‡
Xi'an Jiaotong University, 710049 Xi'an, People's Republic of China

DOI: 10.2514/1.42426

The transmission of external jet noise through the double-leaf skin plate of an aircraft cabin fuselage in the presence of external mean flow is analytically studied. An aeroacoustic–elastic theoretical model is developed and applied to calculate the sound transmission loss versus frequency curves. Four different types of acoustic phenomenon (i.e., the mass–air–mass resonance, the standing-wave attenuation, the standing-wave resonance, and the coincidence resonance) for a flat double-leaf plate as well as the ring frequency resonance for a curved double-leaf plate are identified. Independently of the proposed theoretical model, simple closed-form formulas for the natural frequencies associated with the preceding acoustic phenomena are derived using physical principles. Excellent agreement between the model predictions and the closed-form formulas is achieved. Systematical parametric investigation with the model demonstrate that the presence of the mean flow as well as the sound incidence angles substantially affect the sound transmission behavior of the double-leaf structure. The influences of the panel curvature together with cabin internal pressure on jet noise transmission are also significant and should be taken into account when designing aircraft cabin fuselages.

Nomenclature

c	=	sound speed in air
c_t	=	speed of the flexural bending wave in the panel
c_1	=	speed of the sound in the incident fluid medium
c_2	=	speed of the sound in the middle fluid medium
c_3	=	speed of the sound in the transmitted fluid medium
D	=	flexural rigidity of aeroelastic panel
E	=	Young's modulus of the panel material
f_c	=	coincidence resonance frequency
$f_{d,n}$	=	standing-wave resonance frequency
$f_{p,n}$	=	standing-wave attenuation frequency
f_R	=	ring resonance frequency
f_α	=	mass–air–mass resonance frequency
H	=	depth of the middle fluid medium
h	=	thickness of the single-leaf panel
k_{il}	=	wave-number components ($i = 1, 2, 3$ and $l = x, y, z$)
k_l	=	wave-number components in the x, y, and z directions, respectively ($l = x, y, z$)
k_1^*	=	ω/c_1
M	=	Mach number
m	=	mass per unit area of a single-leaf panel
m_1	=	mass per unit area of the incident panel
m_2	=	mass per unit area of the transmitted panel
P_i	=	amplitude of the incident sound wave
p	=	amplitude of the sound pressure
p_1	=	sound pressure in the incident field
p_2	=	sound pressure in the middle field
p_3	=	sound pressure in the transmission field
R	=	radius of the curved panel
t	=	time variable
$\mathbf{V}$	=	velocity vector of mean flow
v	=	speed of mean flow along the x direction
w_i	=	plate deflection ($i = 1, 2$)
w_{i0}	=	amplitude of plate deflection ($i = 1, 2$)
Z_{p1}	=	incident panel impedance
Z_{p2}	=	transmitted panel impedance
Z_1	=	equivalent characteristic impedance of the incident fluid medium
Z_2	=	equivalent characteristic impedance of the middle fluid medium
Z_3	=	equivalent characteristic impedance of transmitted fluid medium
β	=	azimuth angle of mean flow
β_n	=	amplitudes of the reflected sound pressure wave
ε_n	=	amplitudes of the positive-going sound pressure wave
ζ_n	=	amplitudes of the negative-going sound pressure wave
η	=	loss factor of the panel material
λ	=	sound wavelength in air
$\tilde{\lambda}_j$	=	displacement of fluid particle adjacent to the plate ($j = 1, 2, 3, 4$)
$\tilde{\lambda}_{j0}$	=	amplitude of fluid particle displacement ($j = 1, 2, 3, 4$)
ν	=	Poisson ratio of the panel material
ξ_n	=	amplitudes of transmitted sound pressure wave
ρ_1	=	density of the incident fluid medium
ρ_2	=	density of the middle fluid medium
ρ_3	=	density of transmitted fluid medium
τ	=	transmissivity of the incident sound wave
τ_{diff}	=	averaged transmissivity of the incident sound wave
φ_i	=	elevation angle of the sound wave ($i = 1, 2, 3$)
ω	=	circular frequency

Received 27 November 2008; revision received 21 March 2009; accepted for publication 12 April 2009.

*Ph.D. Candidate, Ministry of Education Key Laboratory for Strength and Vibration, School of Aerospace, fengxian.xin@gmail.com.

†Professor, Ministry of Education Key Laboratory for Strength and Vibration, School of Aerospace, tjlu@mail.xjtu.edu.cn.

‡Professor, Ministry of Education Key Laboratory for Strength and Vibration, School of Aerospace, cchen@mail.xjtu.edu.cn.

I. Introduction

THE reduction of sound transmission in aircraft interiors is a classical structural acoustic topic of paramount importance for the successful development of supersonic (or high subsonic) civil and military aircraft [1–18]. In general, the construction of such aircraft is made by thin-walled structural elements. For example, double-leaf aeroelastic plates with an dissipative layer placed between are commonly used for constructing the aircraft cabin fuselage [1,4–7,15,19–22]. From the vibroacoustic point of view, the use of double-leaf partitions provides much more effective noise insulation over a wide frequency range than do single-leaf plates. The air cavity formed between the outer panel (i.e., the source panel) and the trim panel (i.e., the radiating panel) is usually filled with high-density fiberglass

blankets to improve thermal insulation and noise attenuation. However, the use of fiberglass blankets leads to an increase of weight and thus offsets the preceding benefits to some extent.

Turbulent boundary-layer (TBL)-induced noise and engine exhaust noise have been recognized as the primary sources of the interior noise of aircraft cabins [1,4–6,10,13,14,22–27]. A great deal of work is available concerning the influences of convected fluid loaded on aircraft skin plates. For example, the acoustic power radiated by thin flexible panels subjected to TBL wall-pressure fluctuations was estimated by Davies [28] using a modal analysis method, in which the light fluid loading effects were considered. Also using the method of modal expansion, Dowell [2] theoretically analyzed the transmission of TBL-induced noise through a flexible plate into a closed cavity by accounting for the effects of nonlinear plate stiffness and interaction between the plate and the external airflow.

On the basis of the variational method for the vibration of a plate, a set of formulas for sound radiation from rectangular baffled plates having arbitrary boundary conditions was developed by Berry et al. [29]. This was later extended by Atalla and Nicolas [11] to study inviscid uniform subsonic flow, in which the effects of the fluid flow were explicitly shown in terms of added mass and radiation resistance to avoid integration in the complex domain. Subsequently, by employing a suitable polynomial function to describe the displacement of a fluid-loaded plate having elastic boundary conditions, Berry [30] developed a new formulation for the vibration and sound radiation of the plate.

Based upon the radiation of the sound from a single, flat, elastic plate under TBL excitation, Graham [21] proposed a model to address the design problems associated with aircraft cabins, although the effect of mean flow was not taken in account. Graham [22] then developed an extended model consisting of a boundary-layer-excited flat plate with its interior covered by two dissipative layers to simulate a factual aircraft cabin plate, and found that the presence of the dissipative layers greatly reduces the radiation efficiency compared with a bare plate. A coupled finite element method with boundary element method (FEM–BEM) approach was adopted by Sgard et al. [31] to investigate the effects of the mean flow upon the vibroacoustic behavior of a flat plate subjected to a point force, where it was assumed that the mean flow remains undisturbed by the vibrating plate. The formulation [31] can explicitly show the effects of the mean flow in terms of added mass, damping, and stiffness, as done by Atalla and Nicolas [11]. The dynamic and acoustic responses of a finite baffled plate excited by TBL was investigated by Maestrello [32], in which the effect of structural nonlinearities induced by in-plane forces was considered.

Recently, researchers performed systematical studies on the aeroelastic structural response of a single-leaf panel excited by TBL noise and coupled with full potential flow aerodynamics [8–10,13,33–35]. The model accounting for the aerodynamic loading of the panels and linearized potential flow aerodynamics was first developed in [8], and further analyses with the TBL-induced noise disturbance taken into account were presented in [13,33,34,36]. In addition, numerous numerical, theoretical, and experimental investigations have been devoted to studying the transmission of airborne sound across double-panel partitions immersed in static fluid [5,18–20,37–52].

Most of the aforementioned investigations, however, focus either on the TBL-induced noise transmission or the transmission of the sound from static fluid (irrespective of mean flow), or on the effects of the mean flow on structural stability [i.e., panel flutter and self-excited vibrations (see, for example, Crighton [53] for a list of references)]. Only a few studies [3,10] have specifically considered the influence of the mean flow on external noise transmission, although this is of particular importance for studying jet noise transmission into an aircraft. To squarely address this issue in the present study, we develop an aeroacoustic–elastic theoretical model to quantify the influence of external mean flow on sound transmission through a double-leaf aeroelastic plate. The paper is organized as follows. First, an aeroacoustic–elastic theoretical model to emulate the transmission of jet power or propeller-induced noise into the cabin interior is presented for the sound transmission loss (STL), in which the plate dynamics and fluid–structural coupling are accounted for. Second, the physical mechanisms associated with the sound transmission process are discussed and a set of simple closed-form formulas for the associated natural frequencies is derived from physical principles, independently of the theoretical model. These formulas are then used to validate the model predictions, as no suitable experimental or numerical or theoretical results exist in the open literature that can be used to check the validity of the present model. The effects of a few relevant parameters (e.g., Mach number, direction of mean flow, sound incidence angle, panel curvature, and cabin internal pressure) on the STL are systematically explored. The paper finishes with concluding remarks drawn from the obtained results.

II. Statement of the Problem

To mimic the transmission of engine exhaust noise into the interior of an airplane cabin under typical cruise conditions, a uniform plane sound wave varying harmonically in time is assumed to transmit through a double-leaf aeroelastic plate from the external mean flow side to the interior static fluid side. As shown in Fig. 1, the considered system consists of two infinite parallel flexural plates made of homogenous and isotropic materials and is immersed in inviscid, irrotational fluid media. The upper, middle, and bottom fluid media separated by the two plates occupy the spaces of $z < 0$, $h_1 < H + h_1$, and $z > H + h_1 + h_2$, respectively, and are characterized by (ρ_1, c_1), (ρ_2, c_2), and (ρ_3, c_3) in terms of mass density and sound speed, respectively. Here, H is the depth of the air gap, and h_1 and h_2 are the thicknesses of the two panels. The mean fluid flow with uniform speed v is assumed to move along the x-axis direction. The incident sound wave transmitting from the external mean flow side is characterized by elevation angle φ_1 and azimuth angle β with respect to the defined coordinate system (see Fig. 1). The incident sound is partially reflected and partially transmitted through the structure via the upper plate, middle fluid medium, and bottom plate into the static fluid medium side. The double-layer plate is modeled initially as a flat double-leaf aeroelastic partition, with both the external mean flow and the aeroelastic coupling accounted for. Subsequently, to better emulate the curved skin of an aircraft fuselage and the real process of jet noise penetration into aircraft interior, the effects of the panel curvature and cabin internal pressurization on sound transmission are quantified.

Several simplifying assumptions are adopted in the present analysis of the system shown in Fig. 1:

1) The two plates are modeled by the classical Kirchhoff thin plate theory.

2) The fluid media are inviscid and irrotational [8–11,13,31–35].

3) The plate surface adjacent to the mean flow is sufficiently smooth such that it is appropriate to represent the plate-fluid interface by the streamline of the fluid flow (i.e., the total flow is tangential to the acoustically deformed boundary [3,54]). Note that several previous studies [55–57] also considered the problem of the sound reflection and transmission associated with a moving fluid medium, but without accounting for the interaction with a thin plate.

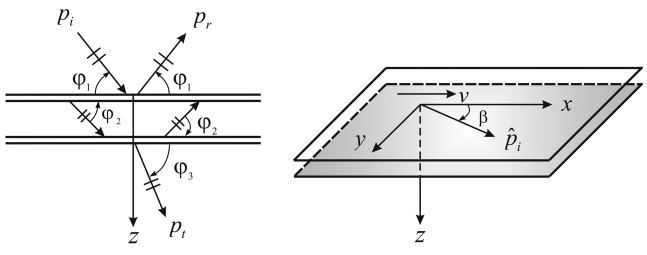

a) **b)**

Fig. 1 Schematic illustration of the sound transmission through a double-leaf aeroelastic plate in the presence of external mean flow: a) side view and b) global view.

III. Theoretical Formulation

A. Formulation of Plate Dynamics

As shown in Fig. 1, the acoustic field is divided into three regimes by the two parallel flat plates that, without loss of generality, are assumed subsequently to have the same thickness. The corresponding sound pressures for the incident field, the middle field, and the transmission field (denoted by indices 1, 2, and 3, respectively) can be expressed as

$$p_1 = P_i e^{i\omega t - i(k_{1x}x + k_{1y}y + k_{1z}z)} + \sum_n \beta_n e^{i\omega t - i(k_{1x}x + k_{1y}y - k_{1z}z)} \tag{1}$$

$$p_2 = \sum_n \varepsilon_n e^{i\omega t - i(k_{2x}x + k_{2y}y + k_{2z}z)} + \sum_n \zeta_n e^{i\omega t - i(k_{2x}x + k_{2y}y - k_{2z}z)} \tag{2}$$

$$p_3 = \sum_n \xi_n e^{i\omega t - i(k_{3x}x + k_{3y}y + k_{3z}z)} \tag{3}$$

The summation index n is introduced in Eqs. (1–3) as a consequence of the modal decomposition of the pressure p_2 onto the standing-wave modes of the cavity, which justifies (through the continuity equations [see Eqs. (17) and (18)]) the present modal formulation for the reflected and the transmitted pressure amplitudes. Note, however, that this index does not appear explicitly through the wave-number components in the argument of the exponential factors. The wave-number components in Eqs. (1–3) can be written as

$$k_{1x} = k_1 \cos\varphi_1 \cos\beta, \qquad k_{1y} = k_1 \cos\varphi_1 \sin\beta, \qquad k_{1z} \sin\varphi_1 \tag{4}$$

$$k_{2x} = k_2 \cos\varphi_2 \cos\beta, \qquad k_{2y} = k_2 \cos\varphi_2 \sin\beta, \qquad k_{2z} \sin\varphi_2 \tag{5}$$

$$k_{3x} = k_3 \cos\varphi_3 \cos\beta, \qquad k_{3y} = k_3 \cos\varphi_3 \sin\beta \qquad k_{3z} = k_3 \sin\varphi_3 \tag{6}$$

Let c_t be the trace wave speed in the plate and let the trace wave number be given by $k_t = \omega/c_t = 2\pi/\lambda_t$, where λ_t is the wavelength of the panel trace wave. Accordingly, the transverse deflections of the two plates induced by the incident sound can be expressed as

$$w_1(x, y; t) = w_{10} e^{i\omega t - i(k_t \cos\beta)x - i(k_t \sin\beta)y} \tag{7}$$

$$w_2(x, y; t) = w_{20} e^{i\omega t - i(k_t \cos\beta)x - i(k_t \sin\beta)y} \tag{8}$$

In the incident acoustic field, there exists a uniform flow of velocity $\mathbf{V}$ tangential to the acoustically deformed boundary (i.e., the fluid–plate interface). The convected wave equation for the pressure in the fluid is then given by [3]

$$\frac{D^2 p_1}{Dt^2} = \left(\frac{\partial}{\partial t} + \mathbf{V}\cdot\nabla\right)^2 p_1 = c_1^2 \nabla^2 p_1 \tag{9}$$

As stated previously, for simplicity, the mean flow is aligned along the x axis on the fluid–plate interface. Consequently, Eq. (9) can be simplified as

$$\left(\frac{\partial}{\partial t} + v\cdot\frac{\partial}{\partial x}\right)^2 p = c_1^2 \nabla^2 p_1 \tag{10}$$

Substituting Eq. (1) into Eq. (10), one obtains the wave number in the flowing fluid as

$$k_1 = \frac{k_1^*}{(1 + M\cos\varphi_1 \cos\beta)} \tag{11}$$

where $k_1^* = \omega/c_1$ is the acoustic wave number in the fluid at rest and $M = v/c_1$ is the Mach number of the mean flow.

Different from the incident field coupled with a mean flow, the fluid medium between the two plates and that in the transmitted field are both static. In such cases, the propagation of the sound obeys the classical wave equation, so that the wave numbers in the two fluid mediums are given by

$$k_2 = \frac{\omega}{c_2}, \qquad k_3 = \frac{\omega}{c_3} \tag{12}$$

For the sound waves to fit at the boundary (i.e., the plate), the trace wavelengths must match [3]: namely,

$$k_{1x} = k_t \cos\beta = k_{2x} = k_t \cos\beta = k_{3x} \tag{13}$$

$$k_{1y} = k_t \sin\beta = k_{2y} = k_t \sin\beta = k_{3y} \tag{14}$$

Incorporating Eqs. (4–6) into Eqs. (13) and (14), one obtains the directions of the sound propagation in the middle and the transmitted fluid mediums as

$$\varphi_2 = \arccos\left(\frac{c_2}{c_1}\frac{\cos\varphi_1}{1 + M\cos\varphi_1\cos\beta}\right) \tag{15}$$

$$\varphi_3 = \arccos\left(\frac{c_3}{c_1}\frac{\cos\varphi_1}{1 + M\cos\varphi_1\cos\beta}\right) \tag{16}$$

which also describe the refraction laws for sound transmission from one medium to another. Note that $\varphi_1 = \varphi_2 = \varphi_3$ and $c_1 = c_2 = c_3$ in the absence of the mean flow ($M = 0$). Thus, one noticeable effect of the mean flow [3] is to refract the wave at the plate. In fact, in the presence of the mean flow, the wave would be refracted (and partially reflected) even if the plates were not present.

B. Consideration of Fluid–Structure Coupling

To determine the unknown parameters appearing in the preceding equations, supplementary boundary conditions are needed (i.e., the displacement continuity condition between the plate particle and the adjacent fluid particle, and the driving relation between the incident sound and the plate dynamic response). In general, the continuity condition for the fluid–structure coupling is described through the velocity of the particles pertaining separately to the fluid medium and the solid medium when the fluid is at rest. In the case of a moving flow, however, the transfer effect of the fluid motion needs to be considered [54], and hence the primary particle displacement continuity should be applied, as described subsequently.

1. *Displacement Continuity Condition*

Let χ_1 and χ_2 separately denote the displacements of the fluid particles in the incident field and the middle field, both adjacent to the upper panel, and let χ_3 and χ_4 separately denote the displacements of the fluid particles in the middle field and the transmitted field, both adjacent to the bottom panel. These displacements should satisfy the Navier–Stokes equation for an inviscid and irrotational fluid: namely,

$$\frac{D^2\chi_1}{Dt^2} = -\frac{1}{\rho_1}\frac{\partial p_1}{\partial z}\bigg|_{z=0}, \qquad \frac{D^2\chi_2}{Dt^2} = -\frac{1}{\rho_2}\frac{\partial p_2}{\partial z}\bigg|_{z=h_1} \tag{17}$$

$$\frac{D^2\chi_3}{Dt^2} = -\frac{1}{\rho_2}\frac{\partial p_2}{\partial z}\bigg|_{z=H+h_1}, \qquad \frac{D^2\chi_4}{Dt^2} = -\frac{1}{\rho_3}\frac{\partial p_3}{\partial z}\bigg|_{z=H+h_1+h_2} \tag{18}$$

For harmonic sound wave excitation, the fluid particle displacements take the form of

$$\chi_j = \chi_{j0} e^{i\omega t - i(k_{1x}x + k_{1y}y)} \quad (j = 1, 2, 3, 4) \tag{19}$$

Substitution of Eqs. (1–3) and (19) into Eqs. (17) and (18) gives the amplitudes of the fluid particle displacements as

$$\lambda_{10} = -\frac{ik_{1z}(P_i - \sum_n \beta_n)}{\rho_1(\omega - \nu k_{Ix})^2} \tag{20}$$

$$\lambda_{20} = -\frac{ik_{2z}(\sum_n \varepsilon_n - \sum_n \zeta_n)}{\rho_2\omega^2} \tag{21}$$

$$\lambda_{30} = -\frac{ik_{2z}}{\rho_2\omega^2}\left(\sum_n \varepsilon_n e^{-ik_{2z}H} - \sum_n \zeta_n e^{ik_{2z}H}\right) \tag{22}$$

$$\lambda_{40} = -\frac{ik_{3z}}{\rho_3\omega^2}\sum_n \xi_n e^{-ik_{3z}H} \tag{23}$$

In view of the wave-number relationships [Eqs. (13) and (14)] and the dynamic deflections of the two plates [Eqs. (7) and (8)], the continuity condition of the particle displacements is given by

$$\lambda_{10} = w_{10} = \lambda_{20}, \qquad \lambda_{30} = w_{20} = \lambda_{40} \tag{24}$$

Substitution of Eqs. (7), (8), and (20–23) into Eq. (24) leads to

$$P_i - \sum_n \beta_n = \frac{\rho_1 c_1 \sin\varphi_2}{\rho_2 c_2 \sin\varphi_1}\frac{1}{1 + M\cos\varphi_1\cos\beta}\left(\sum_n \varepsilon_n - \sum_n \zeta_n\right) \tag{25}$$

$$\sum_n \varepsilon_n - \sum_n \zeta_n = \frac{\rho_2 c_2}{\sin\varphi_2}\dot{w}_{10} \tag{26}$$

$$\sum_n \varepsilon_n e^{-ik_{2z}H} - \sum_n \zeta_n e^{ik_{2z}H} = \frac{\rho_2 c_2 \sin\varphi_3}{\rho_3 c_3 \sin\varphi_2}\sum_n \xi_n e^{-ik_{3z}H} \tag{27}$$

$$\sum_n \xi_n e^{-ik_{3z}H} = \frac{\rho_3 c_3}{\sin\varphi_3}\dot{w}_{20} \tag{28}$$

where $\dot{w}_{10} = i\omega w_{10}$ and $\dot{w}_{20} = i\omega w_{20}$.

2. Driving Relations

The driving relations for the pressure difference across the panel and the panel vibration response can be described as

$$P_i + \sum_n \beta_n - \sum_n \varepsilon_n - \sum_n \zeta_n = Z_{p1}\dot{w}_{10} \tag{29}$$

$$\sum_n \varepsilon_n + \sum_n \zeta_n - \sum_n \xi_n = Z_{p2}\dot{w}_{20} \tag{30}$$

Detailed derivations of Eqs. (29) and (30) are given in Sec. III.D for both the flat and curved aeroelastic plates.

For simplicity, the equivalent characteristic impedances for the three separate fluid mediums associated with the transmission of the sound across the double-leaf plate of Fig. 1 are defined as

$$Z_1 = \frac{\rho_1 c_1}{\sin\varphi_1(1 + M\cos\varphi_1\cos\beta)} \tag{31}$$

$$Z_2 = \frac{\rho_2 c_2}{\sin\varphi_2} \tag{32}$$

$$Z_3 = \frac{\rho_3 c_3}{\sin\varphi_3} \tag{33}$$

It is readily seen that, in addition to being strongly dependent on the intrinsic property of the fluid (i.e., density and sound speed), the equivalent characteristic impedances of the fluid media are also determined by the sound incident angle and flow velocity. Actually, these characteristic impedances reflect the close relationship between the sound pressure and the fluid particle velocity.

C. Definition of the Sound Transmission Loss

The transmissivity $\tau(\varphi_1, \beta)$ is defined to quantify the sound transmission through the double-leaf plate [3] as

$$\tau(\varphi_1, \beta) = \frac{\rho_1 c_1}{\rho_2 c_2}\left|\frac{\sum_n \xi_n}{P_i}\right|^2 \tag{34}$$

where

$$\begin{aligned}\frac{P_i}{\sum_n \xi_n} = \frac{1}{4Z_2 Z_3 \cos(k_{2z}H)}[&(Z_1 Z_{p2} + Z_{p1}Z_{p2})(e^{-i(-k_{2z}+k_{3z})H} \\ &- e^{-i(k_{2z}+k_{3z})H}) + Z_2 Z_{p2}(e^{-i(-k_{2z}+k_{3z})H} + e^{-i(k_{2z}+k_{3z})H}) \\ &+ 2Z_2 Z_3\cos(k_{2z}H) + 2iZ_3 Z_{p1}\sin(k_{2z}H) \\ &+ 2iZ_1 Z_3\sin(k_{2z}H) + 2Z_1 Z_2 e^{-ik_{3z}H}]\end{aligned} \tag{35}$$

Accordingly, the sound transmission loss is defined as a decibel scale of the transmissivity:

$$\mathrm{STL} = -10\log_{10}\tau(\varphi_1, \beta) \tag{36}$$

D. Characteristic Impedance of an Infinite Plate

1. Infinite Flat Plate

Consider an infinite plate immersed in a fluid medium and subjected to a harmonic incident sound excitation on one side. The governing equation for the deflection of the plate is given by

$$D\nabla^4 w + m\frac{\partial^2 w}{\partial t^2} = pe^{i\omega t - i(k_{2x}x + k_{2y}y)} \tag{37}$$

Note that in the present study, the structural loss factor η is accounted for by introducing the complex bending stiffness D [17,18], as

$$D = \frac{Eh^3(1 + j\eta)}{12(1 - \nu^2)} \tag{38}$$

Because the incident sound is harmonic, the deflection of the plate is assumed to take the form of

$$w = w_0 e^{i\omega t - i[(k_t\cos\beta)x + (k_t\sin\beta)y]} \tag{39}$$

where is determined by substituting Eq. (39) into Eq. (37) as

$$w_0 = \frac{p}{D(k_{2x}^2 + k_{2y}^2)^2 - m\omega^2} \tag{40}$$

Accordingly, the panel impedance that determines the relation between the sound pressure and the particle velocity is given by

$$Z_p = \frac{p}{\dot{w}} = \frac{p}{i\omega w_0} = im\omega\left(1 - \frac{D\omega^2}{mc_2^4}\cos^4\varphi_2\right) \tag{41}$$

2. Infinite Curved Plate with Biaxial Membrane Stresses

In reality, the aircraft fuselage skin is a typical shallow cylindrical panel structure with internal pressurization during cruise condition. To better emulate the actual fuselage skin and the real process of jet noise penetration into the aircraft interior, the Donnell–Mushtari shallow cylindrical shell theory [3,58] is adopted. The geometry and coordinates of a shallow cylindrical panel of thickness h under biaxial membrane stresses (i.e., N_x in the x direction and N_y in the y direction) are schematically illustrated in Fig. 2. The governing equation for its lateral deformation w can be expressed as

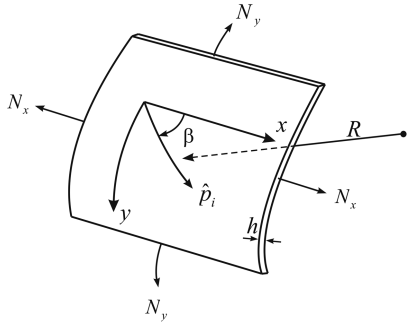

Fig. 2 Shallow cylindrical panel under biaxial membrane stresses.

$$D\nabla^8 w + \frac{Eh}{R^2}\frac{\partial^4 w}{\partial x^4} - \nabla^4\left(N_x\frac{\partial^2 w}{\partial x^2} + N_y\frac{\partial^2 w}{\partial y^2}\right) + m\nabla^4\left(\frac{\partial^2 w}{\partial t^2}\right) = \nabla^4\left(pe^{i\omega t - i(k_{2x}x + k_{2y}y)}\right) \tag{42}$$

After a few algebraic manipulations similar to those leading to Eq. (40), one obtains

$$w_0 = p\cdot\left[D(k_{2x}^2 + k_{2y}^2)^2 + \frac{Eh}{R^2}\frac{k_{2x}^4}{(k_{2x}^2 + k_{2y}^2)^2} + (N_x k_{2x}^2 + N_y k_{2y}^2) - m\omega^2\right]^{-1} \tag{43}$$

which, together with the definition of the panel impedance, leads to

$$Z_p = \frac{p}{\dot{w}} = \frac{p}{i\omega w_0} = \frac{1}{i\omega}\left[D(k_{2x}^2 + k_{2y}^2)^2 + \frac{Eh}{R^2}\frac{k_{2x}^4}{(k_{2x}^2 + k_{2y}^2)^2} + (N_x k_{2x}^2 + N_y k_{2y}^2) - m\omega^2\right] = im\omega\left[1 - \frac{D\omega^2}{mc_2^4}\cos^4\varphi_2 - \frac{Eh}{R^2}\frac{\cos^4\beta}{m\omega^2} - \frac{\cos^2\varphi_2}{mc_2^2}\times(N_x\cos^2\beta + N_y\sin^2\beta)\right] \tag{44}$$

IV. Parametric Study of the Sound Transmission

The primary aims of the parametric study presented subsequently are to investigate how the external mean flow affects the transmission of the sound through a double-leaf aeroelastic plate and to explore the underlying physical mechanisms associated with the airborne sound transmission. For numerical calculation, the physical parameters and structural dimensions of the system are taken as follows. The two plates are both made of aluminum alloy with Young's modulus $E = 70$ GPa, Poisson's ratio $\nu = 0.33$, and loss factor $\eta = 0.01$, typical for the skin panel of a commercial airplane. The plates have the same thickness $h_1 = h_2 = 0.002$ m, and the depth of the air gap is fixed at $H = 0.08$ m. The model developed by Koval [3] for a single-leaf aeroelastic plate is extended to model the fluid medium separated by the two panels, and a wide frequency range from 0 to 10,000 Hz is considered. Air is selected as the sole fluid medium filling all the spaces (see Fig. 1), with density $\rho_1 = \rho_2 = \rho_3 = 1.21$ kg/m^3 and sound speed $c_1 = c_2 = c_3 = 343$ m/s.

A. Physical Interpretation for the Appearance of STL Peaks and Dips

Figure 3 plots the predicted STL as a function of the incident sound frequency for Mach number $M = 0.05$, with the sound incidence elevation angle fixed at $\varphi_1 = 30$ deg and the azimuth angle at $\beta = 0$ deg (i.e., completely aligned with the downstream direction). In Fig. 3, four physical phenomena (i.e., mass–air–mass resonance, standing-wave attenuation, standing-wave resonance, and coincidence resonance) associated with the transmission of the sound from the external mean flow side across the double-leaf partition can be clearly identified, which are marked with symbols in the frequency

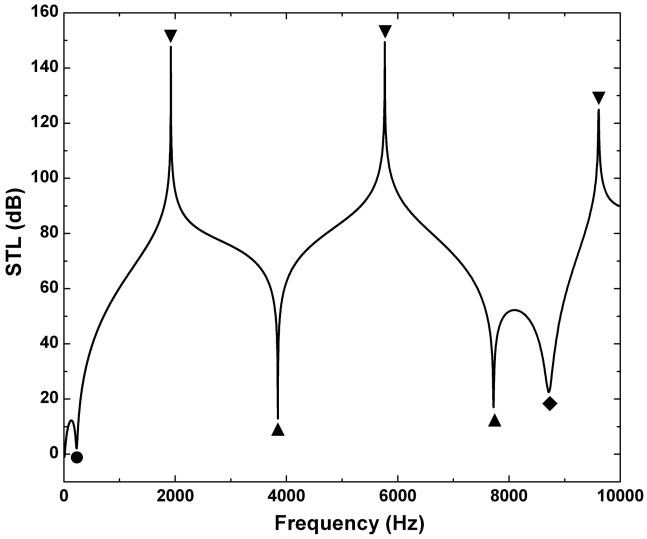

Fig. 3 Predicted STL as a function of frequency for mean flow speed $M = 0.05$, sound incident elevation angle $\varphi_1 = 30$ deg, and azimuth angle $\beta = 0$ deg; ●: mass–air–mass resonance, ▼: standing-wave attenuation, ▲: standing-wave resonance, and ◆: coincidence resonance.

range considered (from 0 to 10,000 Hz). To predict the inherent frequencies associated with these phenomena in the presence of mean flow, a set of simple closed-form formulas are derived based purely on physical principles (see Appendix A). Because the derivation of these formulas is independent of the aeroacoustic–elastic theoretical model presented in Sec. III, they may be used to check the validity of the model predictions, as no other suitable experimental or theoretical work exists. In Fig. 3, the Mach number is selected as $M = 0.05$, only because at this small Mach number, all four physical phenomena can be clearly identified in the considered frequency range of 0–10,000 Hz. Of course, the present model is suitable for handling higher Mach number cases (e.g., $M = 0.4$, 0.8, and 1.2, as shown in Figs. 4–9), although the coincidence resonance occurs beyond 10,000 Hz at large Mach numbers when the sound is incident downstream. Furthermore, when the sound is incident upstream, the three phenomena (i.e., mass–air–mass resonance, standing-wave attenuation, and standing-wave resonance) all disappear, leaving only the coincidence dip in the STL curve (see Fig. 7).

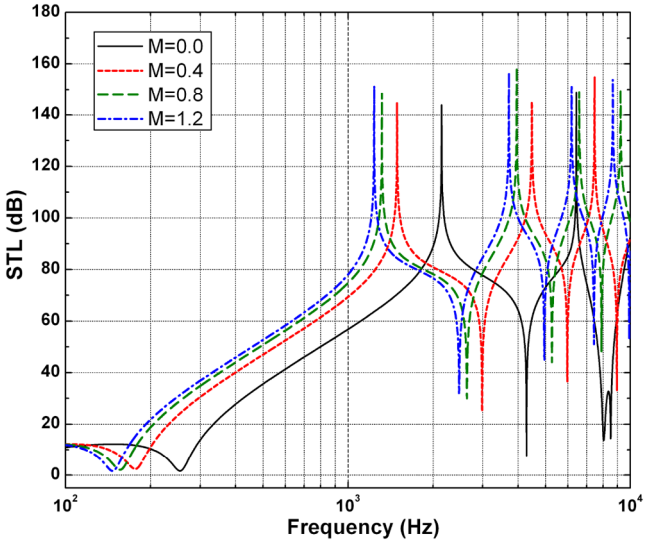

Fig. 4 Predicted STL plotted as a function of frequency for selected Mach numbers with sound incidence elevation angle $\varphi_1 = 30$ deg and azimuth angle $\beta = 45$ deg.

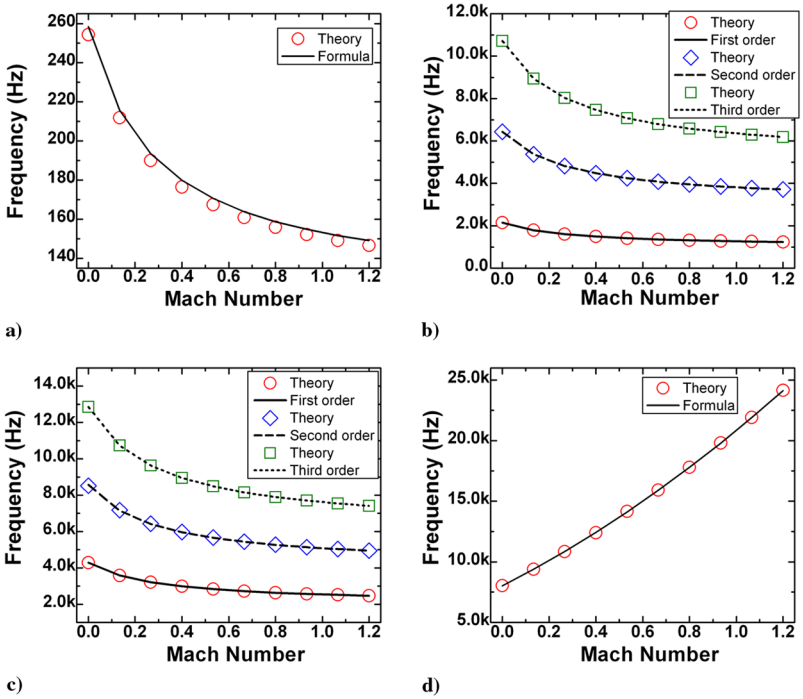

Fig. 5 Effects of Mach number on the frequencies of STL peaks and dips for sound incidence with elevation angle $\varphi_1 = 30$ deg and azimuth angle $\beta = 45$ deg: a) mass–air–mass resonance, b) standing-wave attenuation, c) standing-wave resonance, and d) coincidence resonance. Symbols (e.g., hollow circles, hollow diamonds, and hollow squares) refer to theoretical predictions. Lines (e.g., solid line, dashed line, and dashed-dotted line) denote the calculated results from Eqs. (45–48).

As shown in Fig. 3, the first dip is associated with the mass–air–mass resonance that is marked by the filled circle. The mass–air–mass resonance in the absence of the mean flow usually occurs when the two panels move in opposite phases [17,18,39,46,50], with the air gap behaving like an elastic spring. With the influence of the mean flow accounted for, the frequency of the mass–air–mass resonance is (see Appendix A for detailed derivations):

$$f_\alpha = \frac{1}{2\pi \sin\varphi_2}\sqrt{\frac{\rho_2 c_2^2}{H}\frac{(m_1+m_2)}{m_1 m_2}} \tag{45}$$

In view of the expression for φ_2 in Eq. (15), the preceding relation indicates that f_α is dependent on the Mach number M as well as sound incidence angles φ_1 and β, which is different from that of a double-leaf plate immersed in static fluid.

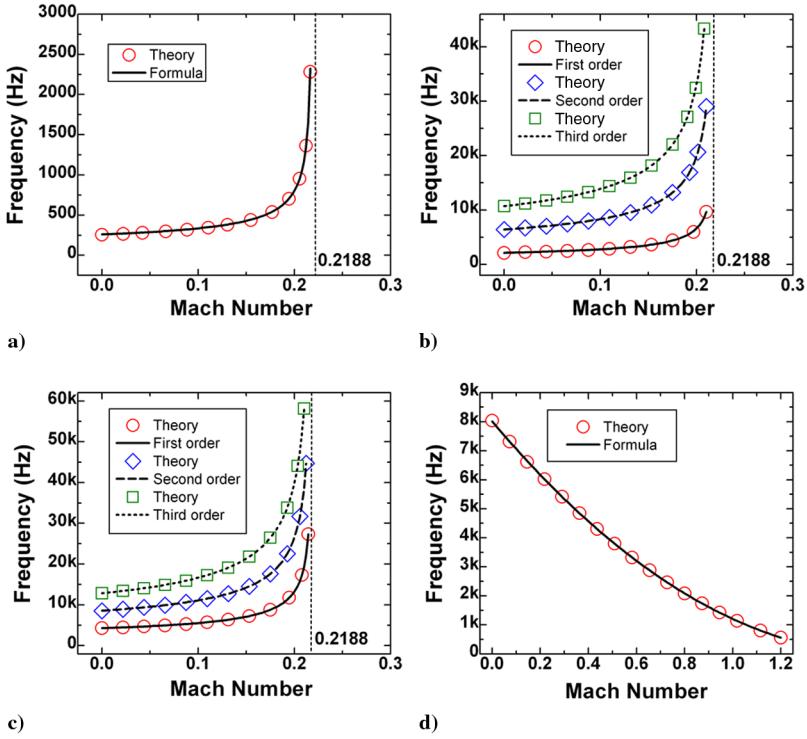

Fig. 6 Effects of Mach number on the frequencies of STL peaks and dips for sound incidence with elevation angle $\varphi_1 = 30$ deg and azimuth angle $\beta = 135$ deg: a) mass–air–mass resonance, b) standing-wave attenuation, c) standing-wave resonance, and d) coincidence resonance.

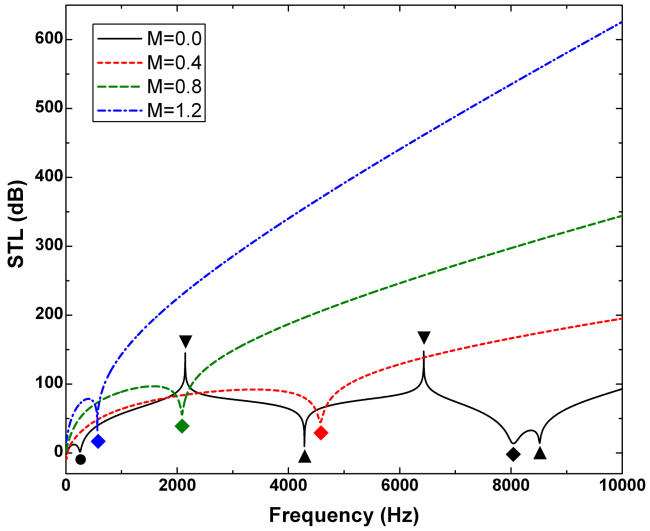

Fig. 7 Variations of STL with incident frequency for selected Mach numbers, with elevation angle $\varphi_1 = 30\,\mathrm{deg}$ and azimuth angle $\beta = 135\,\mathrm{deg}$; ●: mass–air–mass resonance, ▼: standing-wave attenuation, ▲: standing-wave resonance, and ◆: coincidence resonance.

The second phenomenon relates to the three peaks on the STL-vs-frequency curve (marked by the inverted and filled triangle ▼ in Fig. 3), corresponding separately to the first-order, second-order, and third-order standing-wave attenuations. Wave attenuation occurs when the distance difference between the routes that the two intervening waves pass through is odd numbers of one-quarter wavelength of the incident sound. Thus, the frequencies for these standing-wave attenuations are given by (Appendix A)

$$f_{p,n} = \frac{(2n-1)c_2}{4H\sin\varphi_2}, \qquad (n = 1, 2, 3\ldots) \tag{46}$$

which are again dependent upon the Mach number and the sound incidence angles. When standing-wave attenuation occurs, the destructive interference between the positive- and negative-going waves causes the wave amplitude to significantly decrease before the sound is transmitted across the partition, resulting in maximum sound reduction.

In contrast to the standing-wave attenuation, the third phenomenon (i.e., the standing-wave resonance) occurs when the distance difference between the routes that the two intervening waves pass through is multiples of the half-wavelength of the incidence sound (denoted by the filled triangle ▲ in Fig. 3). In such circumstances, the constructive interference of the positive- and negative-going waves leads to an enhanced sound transmission through the partition. The standing-wave resonance as a result of the enhanced effect occurs at the following frequencies (Appendix A):

$$f_{d,n} = \frac{nc_2}{2H\sin\varphi_2}, \qquad (n = 1, 2, 3\ldots) \tag{47}$$

The fourth phenomenon (i.e., the coincidence resonance) occurs when the wavelength of the flexural bending wave in the panel matches the trace wavelength of the incidence sound. The corresponding dip is marked in Fig. 3 by the filled diamond ◆. Because of the influence of the mean flow, the resonance frequency differs from that in the static fluid case, given by (Appendix A)

$$f_c = \frac{c_2^2}{2\pi h\cos^2\varphi_2}\sqrt{\frac{12\rho(1-\nu^2)}{E}} \tag{48}$$

In the absence of mean flow ($M = 0$), according to Eq. (15), the angle φ_2 is equal to the incident angle φ_1 for the case considered here (i.e., $c_1 = c_2$, both panels immersed in air). Consequently, in this limiting case (static fluid), the frequencies for the preceding four phenomena are simply obtained by replacing φ_2 with φ_1 in Eqs. (45–48).

The existence of the four distinct acoustic phenomena significantly influence the shape of the STL-vs-frequency curves, as evidenced by the intense peaks and dips appearing in Fig. 3. The frequencies of the four phenomena predicted from the theoretical model [i.e., Eqs. (1) to (41)] are compared in Table 1 with the closed-form formulas [i.e., Eqs. (45–48)]. Excellent agreement is achieved, which in this way validates the theoretical model, because the closed-form formulas are derived completely independently of the model. Of

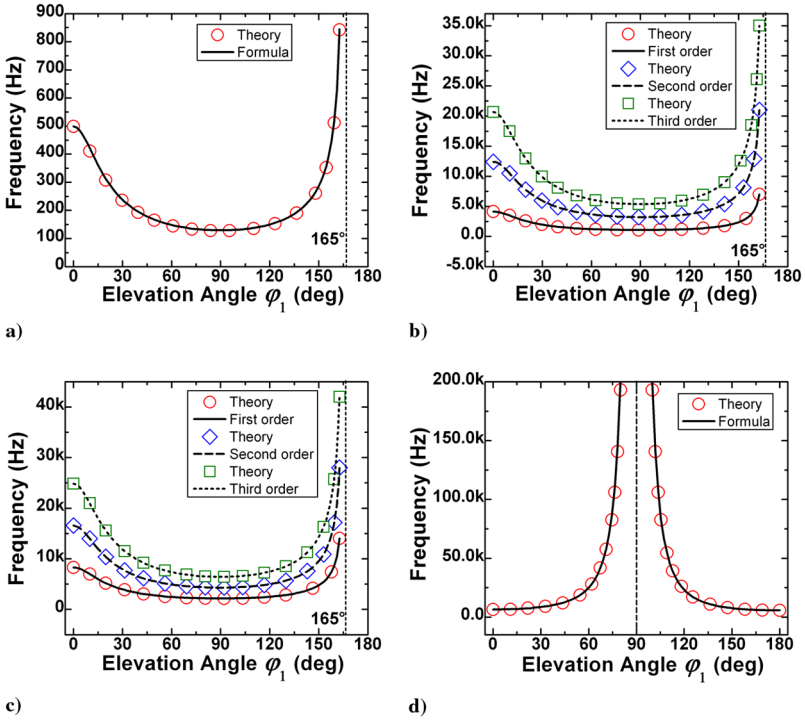

Fig. 8 Effects of the incident elevation angle on the frequencies of STL peaks and dips for sound incidence with azimuth angle $\beta = 45\,\mathrm{deg}$ and Mach number $M = 0.05$: a) mass–air–mass resonance, b) standing-wave attenuation, c) standing-wave resonance, and d) coincidence resonance.

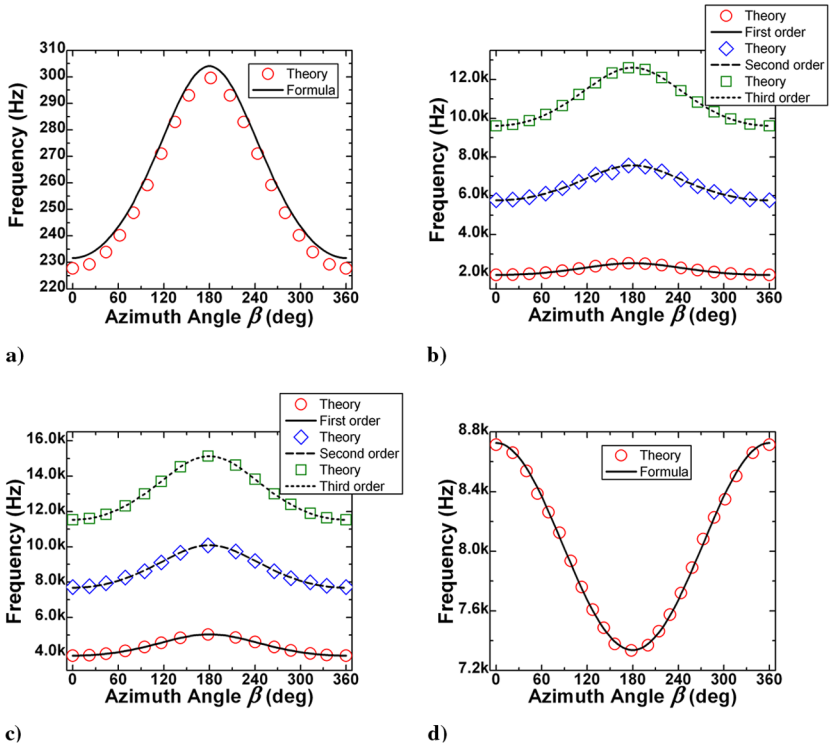

Fig. 9 Effects of the incident azimuth angle on the frequencies of STL peaks and dips for sound incidence with elevation angle $\varphi_1 = 30$ deg and Mach number $M = 0.05$: a) mass–air–mass resonance, b) standing-wave attenuation, c) standing-wave resonance, and d) coincidence resonance.

course, it would be more desirable to validate the present model predictions with other theories or experimental measurements but, unfortunately, none exists in the open literature.

B. Effects of Mach Number

As discussed in the previous section, all four acoustic phenomena associated with the STL peaks and dips depend on the Mach number of the mean fluid flow. It is thus expected that the Mach number plays an important role in the transmission process of the sound through a double-leaf partition. Two typical cases for sound incidence in the downstream direction and in the upstream direction, respectively, are studied subsequently to explore further the Mach number influence.

1. Sound Incidence Along the Downstream Direction

Consider first the case of the sound incidence having an elevation angle of $\varphi_1 = 30$ deg and an azimuth angle of $\beta = 45$ deg, with its wave vector component in the downstream direction being positive. Figure 4 presents the predicted STL-vs-frequency curves for selected Mach numbers, $M = 0$, 0.4, 0.8, and 1.2. It is shown in Fig. 4 that changes in the Mach number lead to noticeable shifts of the STL curves: as the Mach number is increased, the STL peaks and dips are all shifted to lower frequencies, resulting in an increase of the STL value over a relatively broad frequency range. Although the noticeable decrease of the STL peaks and dips can be attributed to the added-mass effect of the convected fluid loading, the increase of the STL value in the frequency range considered agrees well with existing results [10,13]. One may expect that the STL value corresponding to the peaks and dips should also increase as the Mach number is increased, because the aerodynamic damping effect increases when the convected flow becomes more turbulent [10]. However, the increase of the STL value related to the peaks and dips is not as remarkable as anticipated (Fig. 4). This may be attributed to the fact that the present study assumes irrotational, inviscid potential flow, which is much different from the turbulent boundary layer considered by Frampton and Clark [10]. Another possible reason may be that as the Mach number is increased, the complex fluid–structural coupling effects overwhelm the aerodynamic damping effect when the STL peaks and dips move considerably away from their original locations.

By extracting the frequencies associated with the STL peaks and dips for different Mach numbers, the dependence of these frequencies on the Mach number is obtained, as shown in Figs. 5a–5d using different symbols (e.g., hollow circles, hollow diamonds, and hollow squares). For comparison, predictions from the closed-form formulas are also included in Fig. 5, denoted by different lines (e.g., solid line, dashed line, and dashed-dotted line). Note that the first three orders of the frequencies are plotted for the standing-wave attenuation and standing-wave resonance in Figs. 5b and 5c. Similar to the results of Table 1, it is shown in Fig. 5 that the model predictions agree very well with Eqs. (45–48), and the same can be said regarding the other cases shown in Figs. 6, 8, and 9. The results of Fig. 5 demonstrate that except for the coincidence resonance frequencies, the frequencies for the mass–air–mass resonance, standing-wave attenuation, and standing-wave resonance decrease as the Mach number increases, due mainly to the added-mass effects of the convected fluid loading. The exception of the coincidence resonance is attributed to the fact that the significant refraction effect of the mean flow has overwhelmed the added-mass effect on the coincidence resonance.

Table 1 Comparison between theoretical model predictions and simple closed-form formulas for STL peaks and dips ($M = 0.05$, $\varphi_1 = 30$ deg, and $\beta = 0$ deg)

Mass–air–mass resonance f_α, Hz		Standing-wave attenuation $f_{p,n}$, Hz		Standing-wave resonance $f_{d,n}$, Hz		Coincidence resonance f_c, Hz	
Theory	Equation (45)	Theory	Equation (46)	Theory	Equation (47)	Theory	Equation (48)
——	——	1922.2	1922.2	3844.3	3844.3	——	——
227.73	231.69	5766.5	5766.5	7720.5	7688.6	8714.9	8726.2
——	——	9610.8	9610.8	11,533	11,533	——	——

2. Sound Incidence Along the Upstream Direction

Next, consider the case of the sound incidence in the upstream direction, with elevation angle $\varphi_1 = 30$ deg and azimuth angle $\beta = 135$ deg. The effects of the Mach number on the mass–air–mass resonance, the standing-wave attenuation, the standing-wave resonance, and the coincidence resonance frequencies are displayed in Figs. 6a–6d. The frequencies for the first three acoustic phenomena increase with increasing Mach number until a critical value of $M = 0.2188$ is reached, beyond which these phenomena all disappear. The existence of the critical Mach number can be explained as follows. Note from Eqs. (45–47) that $\sin\varphi_2$ is present in each of the denominators and φ_2 depends on the Mach number through Eq. (15). It is shown in Eq. (15) that for sound incidence with $\varphi_1 = 30$ deg and $\beta = 135$ deg, $\sin\varphi_2$ approaches zero as the Mach number approaches 0.2188, thus giving rise to infinitely large values of the frequencies. Consequently, the mass–air–mass resonance, the standing-wave attenuation, and the standing-wave resonance do not exist for $M > 0.2188$. On the other hand, the transmitted evanescent wave for coincidence resonance is enhanced by the coincidence effect of the bottom panel. Accordingly, the corresponding frequency in the present upstream case (see Fig. 6d) decreases as the Mach number is increased, a feature that is opposite to that in the downstream case shown in Fig. 5d.

To further illustrate the shift of the STL peaks and dips with varying flow velocity, Fig. 7 plots the predicted STL-vs-frequency curves for selected Mach numbers, with elevation angle $\varphi_1 = 30$ deg and azimuth angle $\beta = 135$ deg. It is seen that all four acoustic phenomena appear in the case of static fluid ($M = 0$), which are marked by different symbols in Fig. 7. As the Mach number increases, the mass–air–mass resonance, standing-wave attenuation, and standing-wave resonance gradually disappear, consistent with the results of Figs. 6a–6c. This also backs the selection of a small Mach number ($M = 0.05$) for plotting the results in Fig. 3, so that all four different acoustic phenomena can be clearly identified within the considered frequency range. In addition to the disappearing of STL peaks and dips with increasing Mach number, a dramatic increase of the STL value over a broad frequency range is observed in Fig. 7. It should be clarified that the significant increase of the STL value (up to 600 dB) is not only caused by the structural damping, but also by the total reflection phenomenon occurring in the specific case associated with Fig. 7. When total reflection occurs, a disturbance penetrates through the double-leaf panel into the transmitted side fluid medium, and the wave-number component k_z in the z direction takes the form of $-j\hbar$ ($\hbar$ being a positive real number), resulting in a rapid exponential delay of the wave amplitude in the form of $\exp(-\hbar)$. Although the physical nature of the total reflection has been addressed in detail by Ribner [56], we believe that its influence on STL may have been quantified for the first time in Fig. 7.

C. Effects of Elevation Angle

It has been reported that the sound incidence elevation angle has a noticeable effect on the transmission of the sound through a partition immersed in static fluid [46]. For the problem considered here, its influence in the presence of mean flow is quantified. Obtained results for a fixed azimuth angle of $\beta = 45$ deg and a fixed Mach number of $M = 0.05$ are presented in Fig. 8, in which it is seen that the four distinct acoustic phenomena all exhibit significant dependence on the elevation angle. It is interesting to note for the first three phenomena (i.e., the mass–air–mass resonance, the standing-wave attenuation, and the standing-wave resonance) that critical values of the elevation angle exist beyond which all three phenomena instantaneously vanish. For example, for the specific case of $\beta = 45$ deg and $M = 0.05$, the critical value is found to be $\varphi_1 = 165$ deg, whereas for the case of $\beta = 135$ deg and $M = 0.05$ (results not shown here, for brevity), the three phenomena are suppressed when the elevation angle lies within the range between 0 and 15 deg. Moreover, the coincidence resonance frequency becomes infinitely large when the elevation angle approaches $\pi/2$, and the system is symmetrical with respect to the sound incidence angle and the flow direction (e.g., the dependence of the four critical frequencies upon the elevation angle for the case of $\beta = 135$ deg is simply obtained by inverting Fig. 8 for the case of $\beta = 45$ deg).

D. Effects of Azimuth Angle

For sound transmission through sandwich panels with corrugated cores immersed in static fluid, it has been found that the sound incidence azimuth angle β plays a negligible role, due to the symmetrical property of the considered system [18,46]. This is no longer valid, however, if the system is immersed in a flowing fluid. For the present double-leaf plate, Fig. 9 plots the predicted critical frequencies as functions of the azimuth angle β in the specific case of $M = 0.05$ and $\varphi_1 = 30$ deg. The azimuth angle is seen to have a significant effect on all four acoustic phenomena. Note that varying the azimuth angle from 0 to 2π corresponds to four processes in sequence: that is, first downstream phase from 0 to $\pi/2$, first upstream phase from $\pi/2$ to π, second upstream phase from π to $3\pi/2$, and second downstream phase from $3\pi/2$ to 2π. The symmetry of the results shown in Fig. 9 with respect to $\beta = \pi$ is therefore readily understandable. Actually, alteration of these frequencies with respect to the incident azimuth angle confirms the refraction effect of the mean flow.

E. Effects of the Panel Curvature and Cabin Internal Pressurization

As for the investigation of external jet noise penetration through the fuselage skin into the aircraft interior, it would be of great interest to estimate the effects of the panel curvature and cabin internal pressurization on the noise transmission. To this end, we extend Koval's work [3] regarding the effects of the panel curvature and cabin internal pressurization on sound transmission through a single-leaf aeroelastic plate and, for computational simplicity (assuming that the apparent contradiction of an unlimited curved panel can be overlooked), an infinite slightly curved double-leaf panel is considered. However, we believe that the results obtained with this somewhat idealized model are reasonable, because all the physical phenomena have been well captured (as shown subsequently), including the mass–air–mass resonance, the ring frequency resonance, the standing-wave attenuation and resonance, and the coincidence resonance. Particularly, the predicted ring frequency resonance is consistent with existing results [3,59] concerning single-leaf curved panels.

Again, to clearly demonstrate all the significant acoustic phenomena associated with a curved double-leaf panel for frequencies below 10,000 Hz, a small Mach number of $M = 0.05$ is selected, with the incident elevation angle arbitrarily fixed at $\varphi_1 = 30$ deg. Under such conditions, the effects of the panel curvature and internal pressurization are shown in Fig. 10 using a set of combinations: that

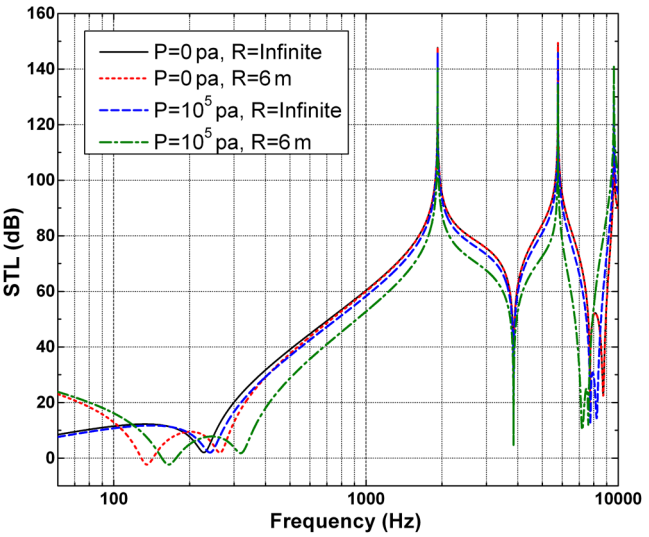

Fig. 10 Effects of the panel curvature and cabin internal pressurization on STL for sound incidence with elevation angle $\varphi_1 = 30$ deg in the presence of external mean flow ($M = 0.05$).

is, a flat panel $R = \infty$ with and without internal pressure $P = 0.1$ MPa and a curved panel $R = 6$ m with and without internal pressure $P = 0.1$ MPa. It is shown in Fig. 10 that, irrespective of the panel curvature or internal pressurization, all four acoustic phenomena can be distinctively identified. In the two cases concerning curved double-leaf panels [i.e., ($P = 0$ Pa and $R = 6$ m) and ($P = 0.1$ MPa and $R = 6$ m)], a newly added ring frequency resonance dip (i.e., the first dip) occurs, which is absent in flat double-leaf panels. In the absence of internal pressure, the ring frequency of the curved panel can be predicted by [3,59]:

$$f_R = \frac{1}{2\pi R}\sqrt{\frac{Eh}{m}} \tag{49}$$

In addition to generating the ring frequency resonance, the panel curvature also shifts the mass–air–mass resonance dip to a higher frequency, which can be seen by comparing the second dip in the curve of ($P = 0$ Pa and $R = 6$ m) with the first dip in the curve of ($P = 0$ Pa and $R = \infty$). Otherwise, the general trend of the STL-vs-frequency curve of the flat panel agrees well with that of the curved panel (Fig. 10).

By comparing the two cases [($P = 0$ Pa and $R = \infty$) and ($P = 0.1$ MPa and $R = \infty$)], it is seen that the internal pressurization shifts the mass–air–mass resonance dip to a higher frequency, but only has a small influence on the second-order standing-wave resonance and coincidence dips. In comparison, the panel curvature has a noticeable influence on all of these phenomena. Therefore, when designing a practical aircraft fuselage, the noticeable combination effects of the panel curvature and internal pressurization on noise transmission need to be carefully considered, especially in the relatively-low-frequency range in which the ring frequency resonance occurs.

V. Conclusions

The effects of external mean flow on sound transmission through double-leaf aeroelastic plates have been quantified analytically, with the intention to simulate the transmission of engine exhaust noise through typical aircraft fuselage skin panels into cabin interiors. Theoretical formulations have been developed for the analysis of the fluid–plate coupling problem, and the STL-vs-frequency curves for various specific cases (Mach number, direction of mean flow, sound incidence angle, panel curvature and internal pressurization) are obtained, with the added-mass effects of the convected fluid loading being well captured. Four distinct acoustic phenomena (i.e., the mass–air–mass resonance, the standing-wave attenuation, the standing-wave resonance, and the coincidence resonance) for flat double-leaf plates as well as the ring frequency resonance for curved double-leaf plates are clearly identified. Simple closed-form formulas for predicting the natural frequencies associated with these acoustic phenomena in the presence of mean flow are subsequently derived from physical principles, which are completely independent of the theoretical model. In the absence of other relevant theoretical or experimental work, the excellent agreement between these formulas and the model predictions serve to validate the two theories against each other.

Systematical parametric studies are subsequently conducted to quantify the effects of Mach number, the direction of mean flow, the sound incidence elevation and azimuth angles, the panel curvature, and the internal pressurization on the STL. As the Mach number is increased, in the case of the sound incidence along the downstream direction, the STL values increase over a broad frequency range and the natural frequencies for the associated acoustic phenomena (except for the coincidence resonance) are shifted considerably to the lower frequency range, due to the added-mass effects of the mean flow. The exception of the coincidence resonance is attributed to its strong dependence on the refraction angle φ_2 but not on the convected fluid loading.

For sound incidence along the upstream direction, the corresponding frequencies increase until the Mach number is increased up to a critical value, again except for the coincidence resonance. Further increase of the Mach number beyond the critical value results in the disappearance of the mass–air–mass resonance, the standing-wave attenuation, and the standing-wave resonance, but the coincidence resonance is always existent. The increase of the Mach number induces a noticeable increment of the STL value over a relatively wide range of frequency due to the total reflection effects.

In the presence of external mean flow, the transmission of the sound is significantly influenced by the sound incidence elevation angle and azimuth angle, and the noticeable combination effects of the panel curvature and internal pressurization should be taken into account in the practical design of aircraft fuselages.

Appendix A: Derivations of Eqs. (45–48) Based Purely on Physical Principles

As stated in Sec. IV, the simple closed-form formulas (45–48) are applied to validate the proposed aeroacoustic–elastic theoretical model in Sec. III, because these formulas are developed independently of the theoretical model. The physical nature of the four acoustic phenomena based on which the closed-form formulas are derived are presented subsequently.

I. Mass–Air–Mass Resonance

In the absence of the external mean flow, the formula for predicting the mass–air–mass resonance frequency of a double-leaf aeroelastic panel has been presented in [16–18,60]. The radially outspreading bending wave in the panel caused by the incident sound leads to the highly directional sound radiation. As a result, the mass–air–mass resonance strongly depends on the incident angle. When the mass–air–mass resonance occurs, the two panels with the air cavity between behave like a mass–spring–mass system, with the stiffness of the air cavity given by $\rho_2 c_2^2/(H\sin^2\varphi_1)$. However, due to the refraction effect of the mean flow, as shown in Fig. A1, the incident angle φ_1 in the presence of the mean flow will be changed to φ_2 before the sound penetrates through the incident panel. In other words, the mean flow case is equivalent to the case when the sound is incident on the panel with angle φ_2 in the absence of the mean flow (denoted by the dashed lines in Fig. A1). Accordingly, the stiffness of the air cavity is changed to $\rho_2 c_2^2/(H\sin^2\varphi_2)$, and the eigenvalue equation of the equivalent mass–spring–mass vibration system becomes

$$\begin{vmatrix} \frac{\rho_2 c_2^2}{H\sin^2\varphi_2} - \omega^2 m_1 & \frac{-\rho_2 c_2^2}{H\sin^2\varphi_2} \\ \frac{-\rho_2 c_2^2}{H\sin^2\varphi_2} & \frac{\rho_2 c_2^2}{H\sin^2\varphi_2} - \omega^2 m_2 \end{vmatrix} = 0 \tag{A1}$$

Solving Eq. (A1) leads to the mass–air–mass resonance given in Eq. (45).

II. Standing-Wave Attenuation

In the presence of external mean flow, the phenomenon of standing-wave attenuation in a double-panel system is caused by the destructive interference between two meeting waves, which occurs only when the distance difference between the routes that the two intervening waves pass through is odd numbers of one-quarter of the incident sound wavelength. Under such conditions, the interference between the positive-gong wave and the negative-going wave tends to be destructive when the sound is transmitting through the partition, resulting in maximum sound reduction. As shown in Fig. A1, the plane sound ray composed of a set of harmonic sound waves with the

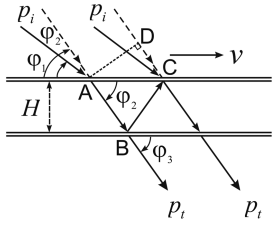

Fig. A1 Sketch of the sound transmission through the double-leaf aeroelastic panel in the presence of external mean flow.

same vibration phase obliquely impinges on the incident panel. There indeed exists a case when one sound ray is incident on the upper panel at point A, transmits through the air cavity onto the bottom panel at point B, and its reflected portion back to the upper panel at poin C meets another sound ray from the external incident side; that is, the interference between the two sound waves has occurred.

As is well known, the destructive effect between two harmonic waves occurs only when their vibration phases differ by odd numbers of $\pi/2$. In the case considered here (Fig. A1), the distance difference between the routes that the two intervening waves pass through is the only cause of the phase difference. For convenience, the equivalent case of the sound incident with angle φ_2 in the absence of mean flow (dashed lines in Fig. A1) is used to represent the case of the sound incident with angle φ_1 in the presence of mean flow (solid lines in Fig. A1). The distance difference between the routes that the two sound waves pass through is such that

$$\overline{AB} + \overline{BC} - \overline{CD} = \frac{2H}{\sin\varphi_2} - 2H\cot\varphi_2\cos\varphi_2 = 2H\sin\varphi_2 \quad \text{(A2)}$$

The occurrence of the destructive effect requires that

$$H\sin\varphi_2 = \frac{(2n-1)\lambda}{4} \quad (n = 1, 2, 3\ldots) \quad \text{(A3)}$$

where $\lambda = c/f$ is the wavelength in air. Equation (46) for the standing-wave attenuation frequency follows from Eq. (A3).

III. Standing-Wave Resonance

As the counterpart of the standing-wave attenuation, the standing-wave resonance is also caused by the interference effect between two meeting waves, which is constructive, however, rather than destructive. It appears when the distance difference between the routes that the two intervening waves pass through is multiples of the half-wavelength of the incidence sound wave. In such cases, the constructive interference between the positive-going and negative-going waves leads to an enhanced transmission through the double-panel partition. The condition for the appearance of the standing-wave resonance is given by

$$H\sin\varphi_2 = \frac{n\lambda}{2} \quad (n = 1, 2, 3, \ldots) \quad \text{(A4)}$$

With the relation $\lambda = c/f$, Eq. (A4) can be readily converted to Eq. (47).

IV. Coincidence Resonance

Similar to the standing-wave attenuation and resonance, the coincidence resonance is also an interference effect between two intervening waves by physical nature. The difference between the two different types of acoustic phenomenon is that the coincidence resonance is caused by wave interference between the sound wave and the panel flexural bending wave. As shown in Fig. A1, there exists a situation when the panel flexural bending wave at point A (excited by the incident sound ray at this point) rapidly outspreads to point C, where it matches another sound ray from the external incident side. The premise for this matching is that the flexural bending wave in the aeroelastic panel propagates faster than sound propagation in air, requiring that the former transmits a larger distance than the later during the same time period (i.e., $\overline{AC} > \overline{DC}$ in Fig. A1), and hence

$$\frac{\overline{AC}}{c_t} = \frac{\overline{DC}}{c} \quad \text{(A5)}$$

This premise is, in general, satisfied in practice. Consequently, the constructive interference between the two waves results in the coincidence resonance. From the governing equation of the panel vibration, we have

$$c_t = \sqrt[4]{\frac{D\omega^2}{m}} \quad \text{(A6)}$$

Substitution of Eq. (A6) and the relation $\overline{DC} = \overline{AC}\cdot\cos\varphi_2$ into Eq. (A5) leads to Eq. (48) for the coincidence resonance frequency.

Note that the coincidence resonance will occur in the bottom panel as well when the upper panel generates coincidence resonance. In other words, the incident sound will be enhanced twice, initially by the upper panel and followed by the bottom panel, when the condition for the occurrence of the coincidence resonance is satisfied.

Acknowledgments

This work is supported by the National Basic Research Program of China (2006CB601202), the National 111 Project of China (B06024), the National Natural Science Foundation of China (10632060 and 10825210), and the National High Technology Research and Development Program of China (2006AA03Z519).

References

[1] Heitman, K. E., and Mixson, J. S., "Laboratory Study of Cabin Acoustic Treatments Installed in an Aircraft Fuselage," *Journal of Aircraft*, Vol. 23, No. 1, 1986, pp. 32–38. doi:10.2514/3.45263

[2] Dowell, E. H., "Transmission of Noise from a Turbulent Boundary Layer Through a Flexible Plate into a Closed Cavity," *Journal of the Acoustical Society of America*, Vol. 46, No. 1B, 1969, pp. 238–252. doi:10.1121/1.1911676

[3] Koval, L. R., "Effect of Air Flow, Panel Curvature, and Internal Pressurization on Field-Incidence Transmission Loss," *Journal of the Acoustical Society of America*, Vol. 59, No. 6, 1976, pp. 1379–1385. doi:10.1121/1.381024

[4] Maury, C., Gardonio, P., and Elliott, S. J., "Model for Active Control of Flow-Induced Noise Transmitted Through Double Partitions," *AIAA Journal*, Vol. 40, No. 6, 2002, pp. 1113–1121. doi:10.2514/2.1760

[5] Gardonio, P., and Elliott, S. J., "Active Control of Structure-Borne and Airborne Sound Transmission Through Double Panel," *Journal of Aircraft*, Vol. 36, No. 6, Nov.–Dec. 1999, pp. 1023–1032. doi:10.2514/2.2544

[6] Alujevic, N., Frampton, K., and Gardonio, P., "Stability and Performance of a Smart Double Panel with Decentralized Active Dampers," *AIAA Journal*, Vol. 46, No. 7, 2008, pp. 1747–1756. doi:10.2514/1.34572

[7] Carneal, J. P., and Fuller, C. R., "Active Structural Acoustic Control of Noise Transmission Through Double Panel Systems," *AIAA Journal*, Vol. 33, No. 4, 1995, pp. 618–623. doi:10.2514/3.12623

[8] Frampton, K. D., Clark, R. L., and Dowell, E. H., "State-Space Modeling for Aeroelastic Panels with Linearized Potential Flow Aerodynamic Loading," *Journal of Aircraft*, Vol. 33, No. 4, 1996, pp. 816–822. doi:10.2514/3.47019

[9] Frampton, K. D., and Clark, R. L., "State-Space Modeling of Aerodynamic Forces on Plate Using Singular Value Decomposition," *AIAA Journal*, Vol. 34, No. 12, 1996, pp. 2627–2630. doi:10.2514/3.13449

[10] Frampton, K. D., and Clark, R. L., "Power Flow in an Aeroelastic Plate Backed by a Reverberant Cavity," *Journal of the Acoustical Society of America*, Vol. 102, No. 3, 1997, pp. 1620–1627. doi:10.1121/1.420073

[11] Atalla, N., and Nicolas, J., "A Formulation for Mean Flow Effects on Sound Radiation from Rectangular Baffled Plates with Arbitrary Boundary Conditions," *Journal of Vibration and Acoustics*, Vol. 117, No. 1, 1995, pp. 22–29. doi:10.1115/1.2873863

[12] Unruh, J. F., and Dobosz, S. A., "Fuselage Structural-Acoustic Modeling for Structure-Borne Interior Noise Transmission," *Journal of Vibration, Acoustics, Stress, and Reliability in Design*, Vol. 110, No. 2, Apr. 1988, pp. 226–233.

[13] Clark, R. L., and Frampton, K. D., "Aeroelastic Structural Acoustic Coupling: Implications on the Control of Turbulent Boundary-Layer Noise Transmission," *Journal of the Acoustical Society of America*, Vol. 102, No. 3, Sept. 1997, pp. 1639–1647. doi:10.1121/1.420075

[14] Grosveld, F., "Plate Acceleration and Sound Transmission Due to

Random Acoustic and Boundary-Layer Excitation," *AIAA Journal*, Vol. 30, No. 3, 1992, pp. 601–607. doi:10.2514/3.10962

[15] Mixson, J. S., and Roussos, L., "Laboratory Study of Add-On Treatments for Interior Noise Control in Light Aircraft," *Journal of Aircraft*, Vol. 20, No. 6, 1983, pp. 516–522. doi:10.2514/3.44902

[16] Xin, F. X., and Lu, T. J., "Effects of Core Topology on Sound Insulation Performance of Lightweight All-Metallic Sandwich Panels," *Materials and Manufacturing Processes* (to be published).

[17] Xin, F. X., and Lu, T. J., "Analytical and Experimental Investigation on Transmission Loss of Clamped Double Panels: Implication of Boundary Effects," *Journal of the Acoustical Society of America*, Vol. 125, No. 3, Mar. 2009, pp. 1506–1517. doi:10.1121/1.3075766

[18] Xin, F. X., Lu, T. J., and Chen, C. Q., "Vibroacoustic Behavior of Clamp Mounted Double-Panel Partition with Enclosure Air Cavity," *Journal of the Acoustical Society of America*, Vol. 124, No. 6, 2008, pp. 3604–3612. doi:10.1121/1.3006956

[19] Alujevic, N., Gardonio, P., and Frampton, K. D., "Smart Double Panel with Decentralized Active Dampers for Sound Transmission Control," *AIAA Journal*, Vol. 46, No. 6, 2008, pp. 1463–1475. doi:10.2514/1.32369

[20] Carneal, J. P., and Fuller, C. R., "An Analytical and Experimental Investigation of Active Structural Acoustic Control of Noise Transmission Through Double Panel Systems," *Journal of Sound and Vibration*, Vol. 272, Nos. 3–5, May 2004, pp. 749–771. doi:10.1016/S0022-460X(03)00418-8

[21] Graham, W. R., "Boundary Layer Induced Noise in Aircraft, Part 1: The Flat Plate Model," *Journal of Sound and Vibration*, Vol. 192, No. 1, 1996, pp. 101–120. doi:10.1006/jsvi.1996.0178

[22] Graham, W. R., "Boundary Layer Induced Noise in Aircraft, Part 2: The Trimmed Flat Plate Model," *Journal of Sound and Vibration*, Vol. 192, No. 1, 1996, pp. 121–138. doi:10.1006/jsvi.1996.0179

[23] Maury, C., Gardonio, P., and Elliott, S. J., "Active Control of the Flow-Induced Noise Transmitted Through a Panel," *AIAA Journal*, Vol. 39, No. 10, 2001, pp. 1860–1867. doi:10.2514/2.1200

[24] Howe, M. S., and Shah, P. L., "Influence of Mean Flow on Boundary Layer Generated Interior Noise," *Journal of the Acoustical Society of America*, Vol. 99, No. 6, 1996, pp. 3401–3411. doi:10.1121/1.414988

[25] Mixson, J. S., and Powell, C. A., "Review of Recent Research on Interior Noise of Propeller Aircraft," *Journal of Aircraft*, Vol. 22, No. 11, 1985, pp. 931–949. doi:10.2514/3.45229

[26] Wilby, J. F., and Gloyna, F. L., "Vibration Measurements of an Airplane Fuselage Structure 1: Turbulent Boundary Layer Excitation," *Journal of Sound and Vibration*, Vol. 23, No. 4, 1972, pp. 443–466. doi:10.1016/0022-460X(72)90503-2

[27] Wilby, J. F., and Gloyna, F. L., "Vibration Measurements of an Airplane Fuselage Structure 2: Jet Noise Excitation," *Journal of Sound and Vibration*, Vol. 23, No. 4, 1972, pp. 467–486. doi:10.1016/0022-460X(72)90504-4

[28] Davies, H. G., "Sound from Turbulent-Boundary-Layer-Excited Panels," *Journal of the Acoustical Society of America*, Vol. 49, No. 3B, 1971, pp. 878–889. doi:10.1121/1.1912428

[29] Berry, A., Guyader, J.-L., and Nicolas, J., "A General Formulation for the Sound Radiation from Rectangular, Baffled Plates with Arbitrary Boundary Conditions," *Journal of the Acoustical Society of America*, Vol. 88, No. 6, 1990, pp. 2792–2802. doi:10.1121/1.399682

[30] Berry, A., "A New Formulation for the Vibrations and Sound Radiation of Fluid-Loaded Plates with Elastic Boundary Conditions," *Journal of the Acoustical Society of America*, Vol. 96, No. 2, 1994, pp. 889–901. doi:10.1121/1.410264

[31] Sgard, F., Atalla, N., and Nicolas, J., "Coupled FEM–BEM Approach for Mean Flow Effects on Vibro-Acoustic Behavior of Planar Structures," *AIAA Journal*, Vol. 32, No. 12, 1994, pp. 2351–2358. doi:10.2514/3.12299

[32] Maestrello, L., "Responses of Finite Baffled Plate to Turbulent Flow Excitations," *AIAA Journal*, Vol. 33, No. 1, 1995, pp. 13–19. doi:10.2514/3.12326

[33] Frampton, K. D., "Radiation Efficiency of Convected Fluid-Loaded Plates," *Journal of the Acoustical Society of America*, Vol. 113, No. 5, 2003, pp. 2663–2673. doi:10.1121/1.1559173

[34] Frampton, K. D., "The Effect of Flow-Induced Coupling on Sound Radiation from Convected Fluid Loaded Plates," *Journal of the Acoustical Society of America*, Vol. 117, No. 3, 2005, pp. 1129–1137. doi:10.1121/1.1852894

[35] Clark, R. L., and Frampton, K. D., "Aeroelastic Structural Acoustic Control," *Journal of the Acoustical Society of America*, Vol. 105, No. 2, Feb. 1999, pp. 743–754. doi:10.1121/1.426265

[36] Frampton, K. D., and Clark, R. L., "Sound Transmission Through an Aeroelastic Plate into a Cavity," *AIAA Journal*, Vol. 35, No. 7, Jul. 1997, pp. 1113–1118. doi:10.2514/2.221

[37] Beranek, L. L., and Work, G. A., "Sound Transmission Through Multiple Structures Containing Flexible Blankets," *Journal of the Acoustical Society of America*, Vol. 21, No. 4, 1949, pp. 419–428. doi:10.1121/1.1906530

[38] London, A., "Transmission of Reverberant Sound Through Double Walls," *Journal of the Acoustical Society of America*, Vol. 22, No. 2, 1950, pp. 270–279. doi:10.1121/1.1906601

[39] Wang, J., Lu, T. J., Woodhouse, J., Langley, R. S., and Evans, J., "Sound Transmission Through Lightweight Double-Leaf Partitions: Theoretical Modeling," *Journal of Sound and Vibration*, Vol. 286, No. 4–5, Sept. 2005, pp. 817–847. doi:10.1016/j.jsv.2004.10.020

[40] Craik, R. J. M., and Smith, R. S., "Sound Transmission Through Double Leaf Lightweight Partitions Part 1: Airborne Sound," *Applied Acoustics*, Vol. 61, No. 2, Oct. 2000, pp. 223–245. doi:10.1016/S0003-682X(99)00070-5

[41] Leppington, F. G., Broadbent, E. G., and Butler, G. F., "Transmission of the Sound Through a Pair of Rectangular Elastic Plates," *IMA Journal of Applied Mathematics*, Vol. 71, No. 6, Dec. 2006, pp. 940–955. doi:10.1093/imamat/hxl017

[42] Chazot, J. D., and Guyader, J. L., "Prediction of Transmission Loss of Double Panels with a Patch-Mobility Method," *Journal of the Acoustical Society of America*, Vol. 121, No. 1, Jan. 2007, pp. 267–278. doi:10.1121/1.2395920

[43] Villot, M., Guigou, C., and Gagliardini, L., "Predicting the Acoustical Radiation of Finite Size Multi-Layered Structures by Applying Spatial Windowing on Infinite Structures," *Journal of Sound and Vibration*, Vol. 245, No. 3, 2001, pp. 433–455. doi:10.1006/jsvi.2001.3592

[44] Kropp, W., and Rebillard, E., "On the Air-Borne Sound Insulation of Double Wall Constructions," *Acustica*, Vol. 85, No. 5, Sept.–Oct. 1999, pp. 707–720.

[45] Antonio, J. M. P., Tadeu, A., and Godinho, L., "Analytical Evaluation of the Acoustic Insulation Provided by Double Infinite Walls," *Journal of Sound and Vibration*, Vol. 263, No. 1, 2003, pp. 113–129. doi:10.1016/S0022-460X(02)01100-8

[46] Xin, F. X., Lu, T. J., and Chen, C., "Sound Transmission Through Lightweight All-Metallic Sandwich Panels with Corrugated Cores," *Advanced Materials Research*, Vols. 47–50, Pts. 1–2, July 2008, pp. 57–60. doi:10.4028/www.scientific.net/AMR.47-50.57

[47] Price, A. J., and Crocker, M. J., "Sound Transmission Through Double Panels Using Statistical Energy Analysis," *Journal of the Acoustical Society of America*, Vol. 47, No. 3A, 1970, pp. 683–693. doi:10.1121/1.1911951

[48] Langley, R. S., Smith, J. R. D., and Fahy, F. J., "Statistical Energy Analysis of Periodically Stiffened Damped Plate Structures," *Journal of Sound and Vibration*, Vol. 208, No. 3, 1997, pp. 407–426. doi:10.1006/jsvi.1997.1150

[49] Sgard, F. C., Atalla, N., and Nicolas, J., "A Numerical Model for the Low Frequency Diffuse Field Sound Transmission Loss of Double-Wall Sound Barriers with Elastic Porous Linings," *Journal of the Acoustical Society of America*, Vol. 108, No. 6, Dec. 2000, pp. 2865–2872. doi:10.1121/1.1322022

[50] Panneton, R., and Atalla, N., "Numerical Prediction of the Sound Transmission Through Finite Multilayer Systems with Poroelastic Materials," *Journal of the Acoustical Society of America*, Vol. 100, No. 1, 1996, pp. 346–354. doi:10.1121/1.415956

[51] Xin, F. X., Lu, T. J., and Chen, C. Q., "Dynamic Response and Acoustic Radiation of Double-Leaf Metallic Panel Partition Under Sound Excitation," *Computational Materials Science* (to be published). doi:10.1016/j.commatsci.2009.04.006

[52] Xin, F. X., Lu, T. J., and Chen, C. Q., "Sound Transmission Through Simply Supported Finite Double-Panel Partitions with Enclosed Air Cavity," *Journal of Vibration and Acoustics* (to be published).
[53] Crighton, D. G., "The 1988 Rayleigh Medal Lecture: Fluid Loading—The Interaction Between Sound and Vibration," *Journal of Sound and Vibration*, Vol. 133, No. 1, 1989, pp. 1–27. doi:10.1016/0022-460X(89)90983-8
[54] Ingard, U., "Influence of Fluid Motion Past a Plane Boundary on Sound Reflection, Absorption, and Transmission," *Journal of the Acoustical Society of America*, Vol. 31, No. 7, 1959, pp. 1035–1036. doi:10.1121/1.1907805
[55] Yeh, C., "Reflection and Transmission of the Sound Waves by a Moving Fluid Laver," *Journal of the Acoustical Society of America*, Vol. 41, No. 4A, 1967, pp. 817–821. doi:10.1121/1.1910411
[56] Ribner, H. S., "Reflection, Transmission, and Amplification of the Sound by a Moving Medium," *Journal of the Acoustical Society of America*, Vol. 29, No. 4, 1957, pp. 435–441. doi:10.1121/1.1908918
[57] Yeh, C., "A Further Note on the Reflection and Transmission of the Sound Waves by a Moving Fluid Layer," *Journal of the Acoustical Society of America*, Vol. 43, No. 6, 1968, pp. 1454–1455. doi:10.1121/1.1911012
[58] Leissa, A. W., *Vibration of Shells*, Acoustical Society of America, Melville, NY, 1993.
[59] Liu, B. L., Feng, L. P., and Nilsson, A., "Sound Transmission Through Curved Aircraft Panels with Stringer and Ring Frame Attachments," *Journal of Sound and Vibration*, Vol. 300, No. 3–5, Mar. 2007, pp. 949–973. doi:10.1016/j.jsv.2006.09.008
[60] Yairi, M., Sakagami, K., Sakagami, E., Morimoto, M., Minemura, A., and Andow, K., "Sound Radiation from a Double-Leaf Elastic Plate with a Point Force Excitation: Effect of an Interior Panel on the Structure-Borne Sound Radiation," *Applied Acoustics*, Vol. 63, No. 7, 2002, pp. 737–757. doi:10.1016/S0003-682X(01)00075-5

J. Wei
Associate Editor